



Deposited via The University of Sheffield.

White Rose Research Online URL for this paper:

<https://eprints.whiterose.ac.uk/id/eprint/144868/>

Version: Published Version

Article:

Maxted, P.F.L., Marsh, T.R., Morales-Rueda, L. et al. (2004) RX J2130.6+4710 - an eclipsing white dwarf-M-dwarf binary star. *Monthly Notices of the Royal Astronomical Society*, 355 (4). pp. 1143-1154. ISSN: 0035-8711

<https://doi.org/10.1111/j.1365-2966.2004.08393.x>

This article has been accepted for publication in *Monthly Notices of the Royal Astronomical Society* ©2004 RAS. Published by Oxford University Press on behalf of the Royal Astronomical Society. All rights reserved.

Reuse

Items deposited in White Rose Research Online are protected by copyright, with all rights reserved unless indicated otherwise. They may be downloaded and/or printed for private study, or other acts as permitted by national copyright laws. The publisher or other rights holders may allow further reproduction and re-use of the full text version. This is indicated by the licence information on the White Rose Research Online record for the item.

Takedown

If you consider content in White Rose Research Online to be in breach of UK law, please notify us by emailing eprints@whiterose.ac.uk including the URL of the record and the reason for the withdrawal request.

RX J2130.6+4710 – an eclipsing white dwarf–M-dwarf binary star

P. F. L. Maxted,^{1,2*} T. R. Marsh,^{3,2} L. Morales-Rueda,^{4,2} M. A. Barstow,⁵
P. D. Dobbie,⁵ M. R. Schreiber,⁶ V. S. Dhillon⁷ and C. S. Brinkworth²

¹*School of Chemistry & Physics, Keele University, Staffordshire ST5 5BG*

²*Department of Physics & Astronomy, University of Southampton, Highfield, Southampton SO17 1BJ*

³*Department of Physics, University of Warwick, Coventry CV4 7AL*

⁴*Department of Astrophysics, Faculty of Science, University of Nijmegen, PO Box 9010, 6500 GL Nijmegen, the Netherlands*

⁵*Department of Physics & Astronomy, University of Leicester, University Road, Leicester LE1 7RH*

⁶*Observatoire de Strasbourg, Université Louis Pasteur, 11 rue de l'Université, 67000 Strasbourg, France*

⁷*Department of Physics and Astronomy, University of Sheffield, Sheffield S3 7RH*

Accepted 2004 September 8. Received 2004 September 2; in original form 2004 July 6

ABSTRACT

We report the detection of eclipses in the close white-dwarf–M-dwarf binary star RXJ2130.6+4710. We present light curves in the *B*, *V* and *I* bands and fast photometry obtained with the three-channel CCD photometer Ultracam of the eclipse in the *u'*, *g'* and *r'* bands. The depth of the eclipse varies from 3.0 mag in the *u'* band to less than 0.1 mag in the *I* band. The times of mid-eclipse are given by the ephemeris $\text{BJD}(\text{mid-eclipse}) = 2\,452\,785.681\,876(2) + 0.521\,035\,625(3) E$, where figures in parentheses denote uncertainties in the final digit. We present medium-resolution spectroscopy from which we have measured the spectroscopic orbits of the M dwarf and white dwarf. We estimate that the spectral type of the M dwarf is M3.5Ve or M4Ve, although the data on which this is based are not ideal for spectral classification. We have compared the spectra of the white dwarf with synthetic spectra from pure hydrogen model atmospheres to estimate that the effective temperature of the white dwarf is $T_{\text{eff}} = 18\,000 \pm 1000$ K. We have used the width of the primary eclipse and duration of totality measured precisely from the Ultracam *u'* data combined with the amplitude of the ellipsoidal effect in the *I* band and the semi-amplitudes of the spectroscopic orbits to derive masses and radii for the M dwarf and white dwarf. The M dwarf has a mass of $0.555 \pm 0.023 M_{\odot}$ and a radius of $0.534 \pm 0.053 R_{\odot}$, which is a typical radius for stars of this mass. The mass of the white dwarf is $0.554 \pm 0.017 M_{\odot}$ and its radius is $0.0137 \pm 0.0014 R_{\odot}$, which is the radius expected for a carbon–oxygen white dwarf of this mass and effective temperature. The light curves are affected by frequent flares from the M dwarf and the associated dark spots on its surface can be detected from the distortions to the light curves and radial velocities. RXJ2130.6+4710 is a rare example of a pre-cataclysmic variable star that will start mass transfer at a period above the period gap for cataclysmic variables.

Key words: binaries: close – binaries: eclipsing – stars: fundamental parameters – stars: individual: RXJ2130.6+4710 – white dwarfs.

1 INTRODUCTION

RXJ2130.6+4710 is a soft X-ray source that was detected in a survey of the galactic plane by the *ROSAT* satellite (Trümper 1983; Motch et al. 1991). Motch et al. (1997) used optical spectroscopy of stars near the position of these X-ray sources to identify and classify optical counterparts in the region of the Cygnus constellation. RXJ2130.6+4710 was identified with a faint star which

they labelled RXJ2130.3+4709 about 12 arcsec SSE of the bright G0 star HD 204906 (=SAO 50947, $V = 8.45$). The spectrum of RXJ2130.6+4710 shows the broad Balmer lines of a typical DA white dwarf together with narrow emission lines in the cores in the Balmer lines and the Ca II H and K lines. Also visible are molecular bands of TiO from the Me-type companion star, which is also the source of the narrow emission lines. They classified RXJ2130.6+4710 as a WD+Me close binary star. Motch et al. report that the radial velocities of broad Balmer lines and emission lines move in opposite directions with an orbital period of approximately 12 h. The white dwarf is too cool to contribute to the X-ray

*E-mail: pflm@astro.keele.ac.uk

flux (1.6×10^{-2} counts s^{-1}), which probably arises from the Me star companion. The distance from the optical counterpart to the catalogued position of the X-ray source is almost exactly the same as the 90 per cent confidence radius of 26.1 arcsec in the position of the X-ray source.

It is likely that RX J2130.6+4710 is the same source as 2E 2128.4+4657, a soft X-ray source detected by the Einstein satellite and identified with HD 204906 by Thompson, Shelton & Arning (1998). The position of 2E 2128.4+4657 given in the Einstein Observatory catalog (Harris et al. 1994) differs by 23 arcsec from the position for the optical counterpart of RX J2130.6+4710 given by Motch et al., which is comfortably within the positional uncertainty of 42 arcsec for the X-ray source. We note that RX J2130.6+4710 appears in the ‘Catalogue of cataclysmic binaries, low-mass X-ray binaries and related objects’ (Ritter & Kolb 1998) as ‘J2130+4710’. The corresponding name in the SIMBAD database (Wenger et al. 2000) is RX J2130.6+4710, which is a more accurate reflection of the position of the optical counterpart ($\alpha = 21^{\text{h}}30^{\text{m}}18^{\text{s}}.6$, $\delta = +47^{\circ}10'08''$, J2000.0) and is the name we use throughout this paper.

White dwarf stars are the remnants of stars less massive than about 5–8 M_{\odot} which have been through the red giant phase of their evolution. The separation of a WD+Me binary with a period of 12 h is 2–3 R_{\odot} , which is much smaller than the typical size of a red giant (~ 100 – $1000 R_{\odot}$). This suggests that RX J2130.6+4710 is a post-common envelope binary (PCEB). In this scenario, the expanding red giant star comes into contact with its Roche lobe and begins to transfer mass to its companion star. This mass transfer is highly unstable, so a common envelope forms around the companion and the core of the red giant. The drag on the companion orbiting inside the common envelope leads to extensive mass loss and dramatic shrinkage of the orbit (Iben & Livio 1993). Common-envelope (CE) evolution affects the evolution of many binary stars and can produce some of the most dramatic objects known, including low-mass and high-mass X-ray binaries, novae, supernovae and AM CVn binaries. However, it is a poorly understood process, so it is useful to study relatively simple PCEBs like RX J2130.6+4710 to see what they can tell us about this phenomenon.

RX J2130.6+4710 is one of a very small sample of eclipsing white dwarfs with companions that can be directly detected in the optical spectrum. These binaries offer a rare opportunity to measure the properties of low-mass stars and white dwarfs accurately. In this paper we report photometric and spectroscopic observations of RX J2130.6+4710. We have used these to measure the masses and radii of the white dwarf and the M dwarf to an accuracy of about 5 per cent. We find that the white dwarf in RX J2130.6+4710 is a typical carbon–oxygen white dwarf and that the M dwarf has a normal radius for its mass.

2 OBSERVATIONS AND REDUCTIONS

2.1 Photometry

We first observed RX J2130.6+4710 using the 1-m Jacobus Kapteyn telescope (JKT) on the Island of La Palma. We obtained 478 images with an *I*-band filter and 520 images with a *V*-band filter using a TEK charge coupled device (CCD) during the interval 1998 August 5–9. The exposure times were 1.5–3 s for the *I*-band images and 1.5–5 s for the *V*-band images. The image scale on the CCD was 0.33 arcsec per pixel. Our intention was to confirm the orbital period of the binary from the sinusoidal reflection effect due to the irradiation of one side of the M dwarf by the white dwarf. We were delighted to

Table 1. Exposure times, T_{exp} , for observations of RX J2130.6+4710 obtained with the JKT. N is the number of useful images obtained.

Filter	N	T_{exp} (s)
<i>U</i>	6	120
<i>B</i>	1002	6.5–60
<i>V</i>	536	30
<i>R</i>	6	20
<i>I</i>	581	30

find that the *V*-band images show an eclipse 0.6-mag deep lasting about 30 m occurring at about 0030UT 1998 August 10. The *I*-band images show an eclipse about 0.1-mag deep at the same time. This is exactly what would be expected for the eclipse of a white dwarf by an M dwarf with a similar luminosity in the *V* band.

We obtained further photometry of RX J2130.6+4710 with the JKT during the interval 2000 August 16–22 using an SITe CCD, which gives the same image scale as the TEK CCD. Images were obtained using Harris *UBVRI* filters. The number of images secured with each filter and the exposure times are given in Table 1. The shorter exposures with the B filter were used for observations during eclipses of RX J2130.6+4710.

Primary eclipses of RX J2130.6+4710 were observed with ULTRACAM and the WHT on the nights of 2002 May 17, 2003 May 24 and 2003 May 25. Attempts to observe the secondary eclipse on 2002 May 19 and 2003 November 13 were compromised by poor seeing and flaring of the M dwarf. We have subsequently discovered that the secondary eclipse is likely to be extremely shallow (see later) so we do not discuss these observations further in this paper.

ULTRACAM is an ultrafast, triple-beam CCD camera. The light is split into three wavelength colours (u' , g' and r' or i') by two dichroic beam-splitters and then passes through a filter. The detectors are three back-illuminated, thinned, Marconi frame-transfer 1024×1024 active area CCD chips with a pixel scale of 0.3 arcsec pixel $^{-1}$. ULTRACAM employs frame transfer CCDs so that the dead time between exposures is negligible (24 msec). Signals from Global Position System (GPS) satellites were used to ensure that the time-stamp for each image is accurate to 1 msec (for further details, see Dhillon & Marsh 2001).

We reduced the data using normal extraction from fixed apertures and also Naylor (1998) optimal extraction from apertures varied in step with the seeing. In the latter case we used aperture radii 1.5 times the full-width at half maximum of the image of RX J2130.6+4710. RX J2130.6+4710 is located only 12 arcsec away from a much brighter G0 star so the photometry can be badly affected in poor seeing. To estimate and correct for the extent of this we placed an aperture on the sky at the same distance from the bright star as RX J2130.6+4710 and symmetrically located with respect to the diffraction spikes from this star.

The bias level in the JKT images was determined from the over-scan regions and was subtracted from the image before further processing. Images of the twilight sky devoid of any bright stars were used to determine flat-field corrections by forming the median image of 3–5 twilight sky images in each filter, one for each night’s data. We used optimal photometry (Naylor 1998) to determine instrumental magnitudes of the stars in each frame. We checked for variability in the stars other than the target star in each frame before calculating differential magnitudes between RX J2130.6+4710 and a comparison star located at $\alpha = 21^{\text{h}}30^{\text{m}}19^{\text{s}}.7$, $\delta = +47^{\circ}10'26''$ (J2000.0). The mean differential magnitudes in the sense (RX J2130.6+4710

Table 2. Apparent magnitudes of RX J2130.6+4710.

<i>U</i>	<i>B</i>	<i>V</i>	<i>R</i>	<i>I</i>	<i>J</i>	<i>H</i>	<i>K_s</i>
14.8	14.9	14.3	13.70	12.2	11.21	10.58	10.36

– comparison) in the *B*, *V* and *I* bands when RX J2130.6+4710 is not in eclipse are -0.74 , 0.29 and 0.21 , respectively.

We used an aperture with a radius of five pixels to measure the instrumental magnitude of RX J2130.6+4710 and the five standard stars in the field of PG 1633+099 with *UBVRI* magnitudes given by Landolt (1992). We used these to calculate the apparent magnitudes for RX J2130.6+4710 given in Table 2. The calibration of our photometry is approximate because the proximity of HD 204906 to RX J2130.6+4710 makes it difficult to measure reliable fluxes. For this reason we only quote one decimal place for our apparent magnitude values. Also given in Table 2 are the infrared apparent magnitudes for RX J2130.6+4710 taken from Hoard et al. (2002).

2.2 Spectroscopy

We observed RX J2130.6+4710 with the 2.5-m Isaac Newton Telescope (INT), also on the island of La Palma, using the IDS spectrograph simultaneously with our JKT observations in 2000 August. Most of our observations were obtained using a narrow slit (0.9–1 arcsec) and a 1200 line mm^{-1} grating on the 235-mm camera with an EEV CCD. The spectra cover the wavelength region 3850–5500 Å at a resolution of about 1.2 Å and the dispersion is about 0.48 Å per pixel. A typical spectrum is shown in Fig. 1. The exposure times were 1200 s and we obtained arc lamp spectra approximately

once per hour to establish the wavelength scale and monitor the spectrograph drift. We also observed one eclipse of RX J2130.6+4710 with the same instrument but with a 300 line mm^{-1} grating and a 4-arcsec wide slit orientated to include the same comparison star used for the JKT photometry. The exposure times were 10 s and there was a 4-s delay between exposures to read out the CCD. The spectra cover the wavelength range 4215–6795 Å at a dispersion of 3.7 Å per pixel.

Extraction of the narrow-slit spectra from the images was performed automatically using optimal extraction to maximize the signal-to-noise of the resulting spectra (Marsh 1989). The arcs associated with each stellar spectrum were extracted using the same weighting determined for the stellar image to avoid possible systematic errors due to the tilt of the spectra on the detector. The wavelength scale was determined from a fourth-order polynomial fit to measured arc line positions. The standard deviation of the fit to the 18 arc lines was typically 1/20 of a pixel. The wavelength scale for an individual spectrum was determined by interpolation to the time of mid-exposure from the fits to arcs taken before and after the spectrum to account for the small amount of drift in the wavelength scale (<0.1 Å) due to flexure of the instrument between arc spectra. We used a spectrum of BD+33 2642 obtained during the same observing run and the tabulated fluxes of Oke (1990) to determine the calibration of counts-to-flux as a function of wavelength in our spectra. No correction for slit losses was attempted but we did correct the spectra for atmospheric extinction. Statistical errors on every data point calculated from photon statistics are rigorously propagated through every stage of the data reduction.

To extract the spectrophotometry taken with a wide slit we summed the measured counts over six spatial pixels centred on the

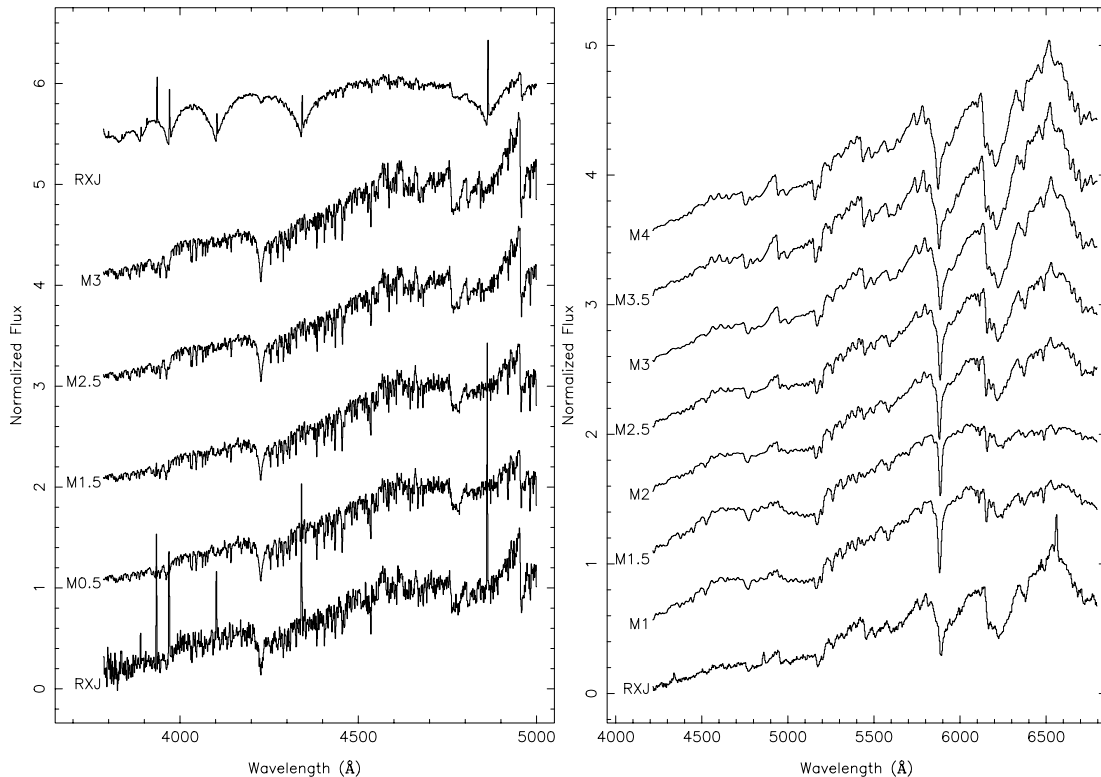


Figure 1. Left panel: from bottom to top – spectrum of RX J2130.6+4710 taken at mid-eclipse, LFT 1580 (M0.5), LFT 1751 (M1.5), LFT 1466 (M2.5), LFT 93 (M3), mean of four spectra of RX J2130.6+4710 taken near phase 0.75. The spectra have been normalized at 5100 Å and offset by 1 for clarity. Right panel: from bottom to top – mean spectrum of RX J2130.6+4710 taken at mid-eclipse, LFT 1278 (M1), LFT 1436 (M1.5), LFT 1580 (M2), LFT 1751 (M2.5), LFT 1466 (M3), LFT 98 (M3.5), LFT 1431 (M4).

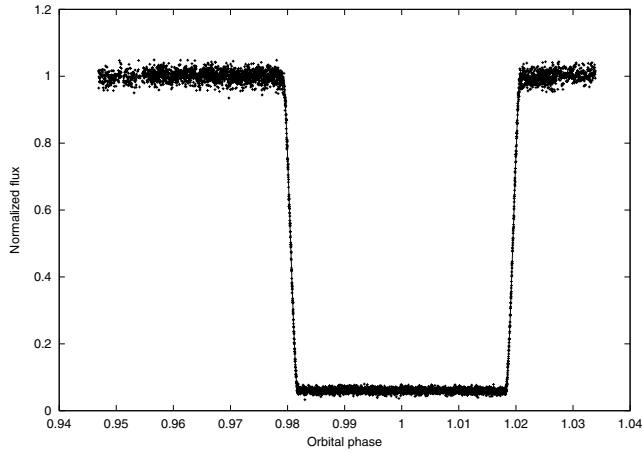


Figure 2. The light curve of RX J2130.6+4710 in the u' band (+) and the least-squares fit for the eclipse of uniform circular discs assuming $i = 80^\circ.5$ (solid line, barely visible).

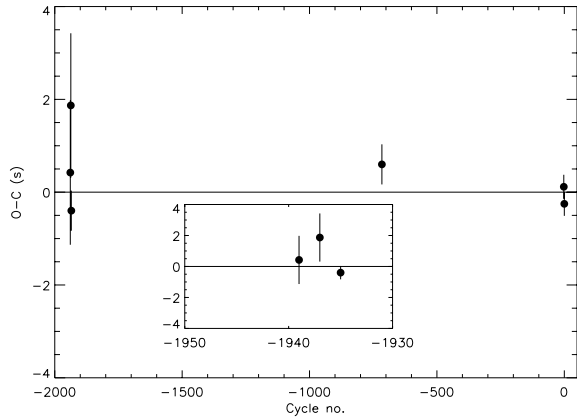


Figure 3. Residuals from a linear ephemeris for our measured times of mid-eclipse.

spectrum at every wavelength step for both RX J2130.6+4710 and the comparison star after subtracting the sky contribution estimated from a linear fit to the regions either side of the spectra. The wavelength calibration was determined from a single arc spectrum taken at the start of the night and is accurate to about 1 Å.

2.3 Timing of INT and JKT data

We warn the reader here that we have not been able to establish whether the time-stamps for the data obtained with the INT and JKT are reliable. It is probable that the time-stamps for these data have an accuracy of better than 1 s. However, the observatory staff have noted that time-stamps on data such as these can be in error by a few seconds.

3 ANALYSIS

3.1 The ephemeris

We measured the time of mid-eclipse from our photometry using a least-squares fit of a very simple light-curve model. The model is based on the eclipse of one circular disc with uniform surface brightness by another similar disc. The parameters of the model are the radii of the discs relative to their maximum separation, r_1 and r_2 ; the inclination of the orbit, i ; the orbital period, P , and time of primary eclipse, T_0 ; the luminosity ratio, l_λ ; the observed inten-

Table 3. Times of mid-eclipse for RX J2130.6+4710.

BJD(mid-eclipse)	Cycle	Source
$245\,1775.393803 \pm 0.000018$	-1939	JKT ^a
$245\,1776.435891 \pm 0.000018$	-1937	JKT ^a
$245\,1777.477936 \pm 0.000005$	-1935	INT ^a
$245\,2412.620375 \pm 0.000005$	-716	Ultracam
$245\,2784.639806 \pm 0.000003$	-2	Ultracam
$245\,2785.681873 \pm 0.000003$	0	Ultracam

^aThese data are not suitable for long-term period studies.

sity outside of eclipse, I_0 , and the mass ratio, q . We also include a parameter to allow for a linear variation of the observed intensity with time. As we were only interested in the time of mid-eclipse, we fixed the parameters $q = 1$, $i = 90^\circ$, $P = 0.52104$ d and found the optimum values of the other parameters using the Levenberg–Marquardt method (Press et al. 1992). We fitted data covering each eclipse we had observed separately. The quality of the fits judged by eye and from the value of χ^2 was very good (Fig. 2). The results are shown in Table 3. Corrections from UTC to Barycentric Julian date (BJD) were calculated using routines from SLALIB v. 2.4–5 (Wallace 2000). The times of mid-eclipse labelled ‘JKT’ are from B -band photometry taken with the JKT with uncertainties derived from the covariance matrix of the least-squares fit. The light curve for the time of mid-eclipse labelled ‘INT’ was produced by summing the total counts over the wavelengths 4215–6796 Å in our low-resolution spectra of RX J2130.6+4710 and the comparison then taking the ratio of these time-series. The uncertainty was also taken from the covariance matrix of the least-squares fit. The times of minimum labelled ‘Ultracam’ are the weighted averages of the values derived by fitting the u' , g' and i' light curves observed with Ultracam. There is an obvious flare during the eclipse observed on 2002 May 17 so we have excluded data in the range JD = 245 2412.632 to 245 2412.635 from the least-squares fit. The uncertainties for these values are taken from the standard deviation of the three measurements. The measurements from the three light curves are consistent with the individual uncertainties taken from the covariance matrix of the least-squares fit. We re-iterate our warning here that timing of the data taken with the INT and JKT presented here may be in error by a few seconds, so *these data should not be used to study the long-term period changes*.

A least-squares fit to these data gives the following linear ephemeris:

$$\begin{aligned} \text{BJD}(\text{Mid-eclipse}) = & (245\,2785.681\,876 \pm 0.000\,002) \\ & + (0.521\,035\,625 \pm 0.000\,000\,003)E. \end{aligned}$$

All phases quoted in this paper have been calculated with this ephemeris. Residuals from this ephemeris for our eclipse timings are shown in Fig. 3.

3.2 Spectral type of the M dwarf

One of our blue narrow-slit spectra was taken during a total eclipse of RX J2130.6+4710 so it only contains light from the M dwarf. This spectrum is compared with spectra of K and M dwarfs taken with the same instrument and setup in Fig. 1. Also shown in Fig. 1 is the average of our wide-slit spectra taken during eclipse compared with spectra of M dwarfs observed with the same instrument and setup. Spectral types for the M dwarfs were taken from Reid, Hawley & Gizis (1995) or Hawley, Gizis & Reid (1996). We estimate that the spectral type of the M dwarf in RX J2130.6+4710 is M3.5 or

M4, based principally on the strength of the TiO bands at 5448, 5847 and 6158 Å and the CaOH band at 5500–5560 Å (Jaschek & Jaschek 1987). The spectra we have used for classification do not cover the TiO bands further to the red, which are more commonly used for spectral classification, and we have used only a few stars that are not standards for the comparison so the uncertainty in the classification is likely to be at least one sub-type.

3.3 Spectroscopic orbit of the M dwarf

We used cross-correlation to measure the radial velocity of the M dwarf from the INT spectra taken in 2000 August. We first removed the contribution of the broad wings of the H β and H γ lines from the white dwarf by using two Gaussian profiles to model each line. The sum of these broad Gaussian profiles and a low-order polynomial was fitted to each spectrum by least squares and then subtracted from the spectrum prior to performing the cross-correlation.

We used spectra of four different M dwarfs taken with the same instrumental setup as templates for the cross-correlation after normalization using a low-order polynomial fit by least-squares. The spectra were re-binned on to a uniform wavelength grid of 1835 pixels of 32 km s⁻¹ each centred on 4600 Å. The cross-correlation function was calculated excluding 10 Å around the two Balmer lines, which are affected by the emission lines from the cool star and the core of the spectral lines from the white dwarf. The radial velocity and its uncertainty were measured from the cross-correlation function using the method of Schneider & Young (1980) – which, briefly, determines the centroid of the CCF weighted in this case by a Gaussian function with a full width at half maximum (FWHM) of 200 km s⁻¹.

We used a least-squares fit to the measured radial velocities, V_r , of the function $V_r = \gamma_M + K_M \sin[2\pi(T - T_0)/P]$ to measure the semi-amplitude of the spectroscopic orbit for the M star, K_M . The values of T_0 and the orbital period, P , were fixed using the ephemeris described in Section 3.1. From inspection of the residuals from these fits it was clear that there was some distortion to the radial velocities with an amplitude of a few km s⁻¹. The residuals tended to be positive over the phases $(T - T_0)/P = 0.2$ – 0.4 and negative over the phases 0.4 – 0.6 . We suspect that this distortion is due to a dark spot on the M dwarf. We do not believe this distortion is a direct consequence of the irradiation of the M dwarf by the white dwarf because such a distortion would be symmetrical around phase 0.5. To model this distortion we add the term $A \sin[(\phi - \phi_0)/\rho]$ to data in the phase range $\phi_0 < \phi < \phi_0 + \rho$, where $\phi = 2\pi(T - T_0)/P$. There may be a similar distortion near phase 0.9, but the data near this phase range is rather sparse so we have decided not to use a more complicated function to fit these data. The physical origin of

this distortion is a dark spot crossing the observer’s meridian on the visible disc of the M dwarf at phase ϕ_{mid} . The velocity of the spot will vary as $\sin(\phi - \phi_{\text{mid}})$ and, since the inclination of the system is approximately 90° its visibility will vary approximately as $\cos(\phi - \phi_{\text{mid}})$. The combination of these effects yields a distortion of the form $\sin(\phi - \phi_{\text{mid}}) \cos(\phi - \phi_{\text{mid}}) = \sin[2(\phi - \phi_{\text{mid}})]$. The effect of limb darkening will be to reduce the time-scale of the variation whereas the finite size of the spot tends to increase the time-scale of the distortion, so that the velocity distortion is approximately $B \sin[(\phi - \phi_{\text{mid}})/\rho]$ with $\rho \approx 0.5$. Note that $\phi_{\text{mid}} = \phi_0 + \rho/2$ so $A = -B$.

The value of χ^2 for these least-squares fits was still rather large. We therefore added an ‘external error’, σ_{sys} , in quadrature to the standard errors of the radial velocity measurements to account for additional sources of uncertainty. These might be instrumental, e.g. motion of the star in the slit, or intrinsic to the M dwarf, e.g. weak emission lines, or spectral features associated with chromospheric activity such as flares or dark spots in the photosphere. The value of σ_{sys} was chosen to obtain a reduced χ^2 value of 1.

The results of the least-squares fit of the sine wave + distortion are given in Table 4. Results are given for each of the templates used for cross-correlation as listed in column 1. The value of γ_M has been corrected for the measured radial velocity of the template, V_{temp} , taken from Nidever et al. (2002). The spectral type of the template taken from Reid et al. (1995) or Hawley et al. (1996) is also given. The standard deviation of the residuals, σ is given in the final column. An example of the measured radial velocities and the function fitted by least-squares is shown in Fig. 4.

We adopt the weighted mean values from Table 4 of $\gamma_M = 15.3 \pm 0.7$ km s⁻¹ and $K_M = 136.4 \pm 0.8$ km s⁻¹. The uncertainties are the standard deviations of the four measurements with a small additional uncertainty in K_M to allow for the partial correlation of K_M with A . These values are both about 1.5 km s⁻¹ lower than that obtained by fitting a simple sine wave to the data.

3.4 Spectroscopic orbit of the white dwarf

The measurement of the radial velocities for the white dwarf in RX J2130.6+4710 was difficult because there are only three spectral lines available to us which show a sufficiently sharp core to give reliable measurements. These spectral regions all show many sharp absorption lines and a strong, variable emission line from the M dwarf. Fortunately, we have a spectrum of the M dwarf alone obtained during an eclipse of the white dwarf. We are able to remove much of the contribution of the M dwarf by subtracting this spectrum from the others. To do this, we first shift the wavelength scale of all the spectra to remove the orbital motion of the M dwarf

Table 4. Results of least-squares fits of a sine wave plus a distortion to the measured radial velocities of the M dwarf in RX J2130.6+4710.

Template (Sp. type)	V_{temp} (km s ⁻¹)	γ_M (km s ⁻¹)	K_M (km s ⁻¹)	A (km s ⁻¹)	ϕ_0	ρ	σ_{sys} (km s ⁻¹)	σ (km s ⁻¹)
LFT 1580 (M0.5)	-17.161	15.6 ±0.7	135.7 ±0.7	2.9 ±0.8	0.18 ±0.04	0.42 ±0.07	3.4	4.5
LFT 1751 (M1.5)	-27.317	15.5 ±0.7	136.4 ±0.7	2.9 ±0.9	0.20 ±0.03	0.40 ±0.06	3.8	4.7
LFT 1466 (M2.5)	35.880	16.1 ±0.7	136.7 ±0.7	2.8 ±0.9	0.23 ±0.04	0.37 ±0.07	3.9	4.8
LFT 93 (M3)	1.500	13.9 ±0.7	136.7 ±0.7	2.8 ±0.9	0.21 ±0.04	0.38 ±0.06	4.0	4.8

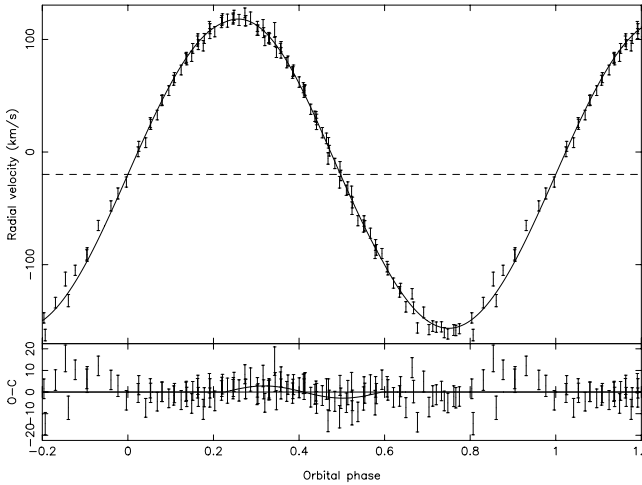


Figure 4. Radial velocities for the M star in RXJ 2130.3+4709 measured by cross-correlation using the spectrum of LFT 1536. The upper panel shows the least-squares fit to the velocities described in the text (sine wave + distortion). The lower panel shows the residuals from the sine wave fit and the function fit by least-squares that is used to model the distortion.

according to the orbit derived in Section 3.3. The spectra were normalized by a constant value determined from the mean flux in the line wings. We interpolated the spectra on to three wavelength grids centred on each of the Balmer lines of 120 pixel of 32 km s^{-1} each. We then formed the average of spectra in groups taken at the same orbital phase to within 0.02 phase units.

We then subtracted from these 47 phase-binned spectra the spectrum obtained in eclipse scaled by some factor so as to optimize the removal of the sharp absorption features. This was done independently for each Balmer line as the optimum factor varies strongly with wavelength. For the $H\delta$ line we found that the spectrum obtained in eclipse was too noisy, so we used the combined spectrum of the M3 and M3.5 dwarfs LFT 1431 and LFT 1432 instead, which looked very similar but was much less noisy. The resulting spectra show a strong absorption line near the line centre and the broad lines of the white dwarf with a weak core whose position varies

sinusoidally with phase. In addition, some spectra show weak emission lines from the M dwarf away from the line centre (Fig. 5) and the stronger central emission line from the M dwarf, which is not entirely removed by the subtraction process.

To measure the radial velocity of the white dwarf from these spectra, we created a model line profile for the white dwarf from the sum of three Gaussian profiles with the same mean but independent widths and depths. We then used least-squares fitting to the phase-binned spectra to determine the widths and depths of these Gaussians. Other parameters in the fit were the coefficients of a linear polynomial used to model the continuum and the width, height and position of a Gaussian used to model the emission line from the M dwarf. Finding the optimum parameters for the Gaussians and the best scaling factor for the M dwarf took much experimentation, but the quality of the fits achieved judged by the χ^2 value and by eye is good. For the measured radial velocities reported here, we fixed the widths and depths of the Gaussians used to model the white dwarf spectrum to be the same for all the spectra. We then repeated least-squares fitting to find the radial velocity of the white dwarf and the other free parameters of the fit. We also corrected for the shift applied to the spectra to correct them for the orbital motion of the M dwarf. The phase-binned spectra around the $H\beta$ line, the model spectra and the residuals from the fit are shown in Fig. 5. Two phase-binned spectra of $H\beta$ observed near quadrature and the model spectra are also plotted in Fig. 6.

We used a least-squares fit to the measured radial velocities, V_r , of the function $V_r = \gamma_{\text{WD}} - K_{\text{WD}} \sin [2\pi(T - T_0)/P]$ to measure the semi-amplitude of the spectroscopic orbit for the white dwarf, K_{WD} . The values of T_0 and the orbital period, P , were fixed using the ephemeris derived in Section 3.1. Note that $\gamma_{\text{WD}} \neq \gamma_{\text{M}}$ for three reasons: (i) the gravitational redshift of light from the white dwarf, $z = 0.635(M/M_{\odot})/(R/R_{\odot}) \text{ km s}^{-1} \approx 25 \text{ km s}^{-1}$; (ii) the Stark effect is asymmetrical for the higher Balmer lines resulting in pressure shifts (Grabowski, Halenka & Madej 1987); (iii) a tilt in the continuum will result in a systematic error in the value of γ_{WD} measured from such broad lines. The resulting fit for the $H\beta$ line is shown in Fig. 7. Also shown are the radial velocities measured for the emission line, which are a by-product of the analysis. The values of γ_{WD} and K_{WD} measured from each Balmer line are given in Table 5. The agreement between the values of K_{WD} measured

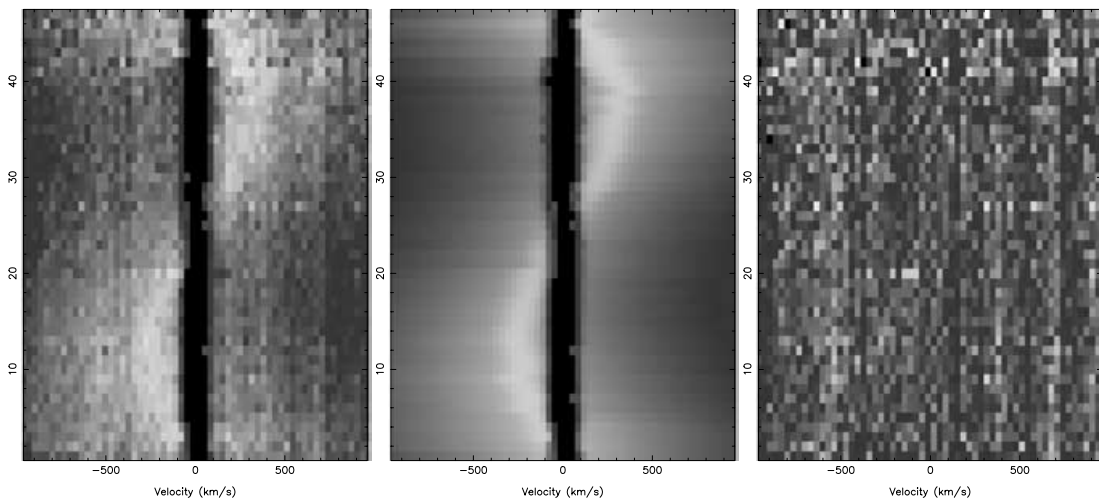


Figure 5. Triled grey-scale spectra of the $H\beta$ line in RXJ2130.6+4710. Left to right: observed, phase binned spectra after subtraction of the M-dwarf spectrum; least-squares fit; residuals from the fit. For the spectra, white is an intensity value of 0.5, black is 1.0. For the residuals, the intensity scale is -0.1 to $+0.1$ from white to black.

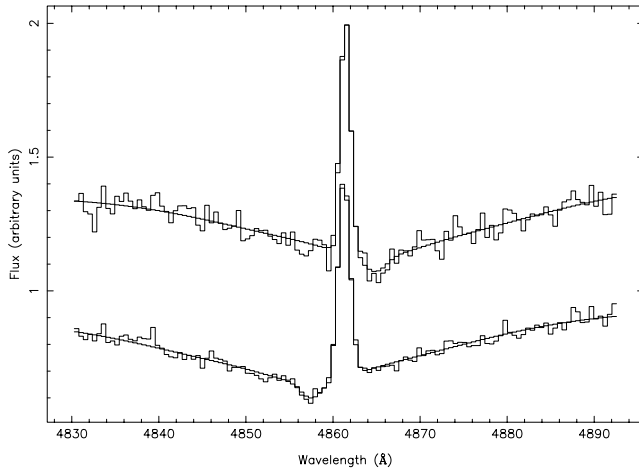


Figure 6. Examples of multiple Gaussian least-squares fits to the $H\beta$ line. Two spectra of RX J2130.6+4710 which have had the M-star spectrum subtracted offset by 0.4 units are shown (thin line) together with the model spectra (thick line).

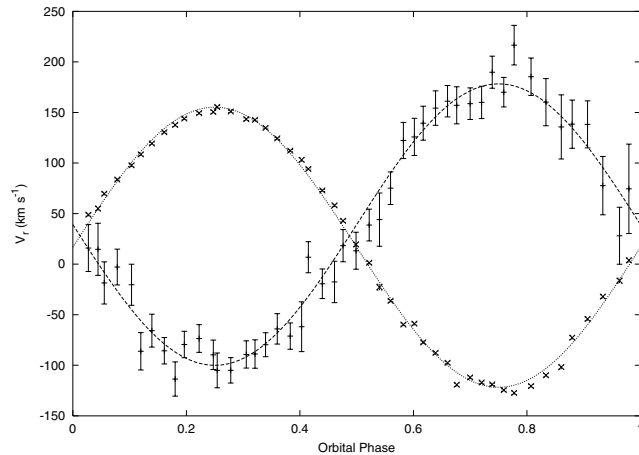


Figure 7. Radial velocities of the white dwarf (+) and the emission line from the M dwarf (x) measured from the $H\beta$ line. Sinusoidal least-square fits are shown as solid lines.

Table 5. Results of least-squares fits of a sine wave to the measured radial velocities of the white dwarf in RX J2130.6+4710.

Spectral line	γ_{WD} (km s^{-1})	K_{WD} (km s^{-1})	χ^2 ($n = 47$)	σ (km s^{-1})
$H\beta$	39.2 ± 2.6	139.2 ± 3.4	43.0	17.9
$H\gamma$	58.4 ± 2.7	133.9 ± 3.8	43.1	21.4
$H\delta$	51.7 ± 2.9	135.5 ± 4.1	52.7	22.3

from the three lines is remarkably good, but we suspect this is a fluke. These values are certainly affected by systematic errors due to inaccurate subtraction of the M-dwarf spectrum, variable tilts in the spectrum and weak emission lines from the M dwarf. Therefore, we should not take the error in the weighted mean as a measure of the uncertainty. Instead we use the standard deviation of the values and adopt the value $K_{\text{WD}} = 136.5 \pm 3.8 \text{ km s}^{-1}$.

Table 6. The combined spectroscopic orbit of RX J2130.6+4710.

Parameter	Value	Notes
T_0	BJD 2 452 785.681876	See Section 3.1
P	0.521 035 625 d	See Section 3.1
γ_{WD}	40 km s^{-1}	Uncertain
K_{WD}	$136.5 \pm 3.8 \text{ km s}^{-1}$	
γ_{M}	$15.3 \pm 0.7 \text{ km s}^{-1}$	
K_{M}	$136.4 \pm 0.8 \text{ km s}^{-1}$	
$q = m_{\text{M}}/m_{\text{WD}}$	1.00 ± 0.03	
$m_{\text{WD}} \sin^3 i$	$0.548 \pm 0.016 M_{\odot}$	
$m_{\text{M}} \sin^3 i$	$0.549 \pm 0.022 M_{\odot}$	
$a \sin i$	$2.81 \pm 0.04 R_{\odot}$	

3.5 The combined spectroscopic orbit

From the adopted value of P , K_{M} and K_{WD} we use Kepler's Law to derive the minimum masses, $m_{\text{M}} \sin^3 i$ and $m_{\text{WD}} \sin^3 i$, the mass ratio $q = m_{\text{M}}/m_{\text{WD}}$, and projected semi-major axis $a \sin i$, where m_{M} is the mass of the M dwarf, m_{WD} is the mass of the white dwarf and i is the orbital inclination. The values derived and their uncertainties are given in Table 6. We have taken the value of γ_{WD} derived from the $H\beta$ line as we believe this to be the least affected but systematic errors.

3.6 The light curve

The light curve of RX J2130.6+4710 shows that the white dwarf is eclipsed for 27 min 30 s and that the ingress and egress phases of the eclipse lasted for 1 min 50 s. The depth of the eclipse varies from 3.0 mag in the u' band to less than 0.1 mag in the I band (Fig. 8). There is no secondary eclipse apparent in our data, which is unsurprising given that it is expected to be less than 1 milli-magnitude deep. It is also noticeable that the amplitude of the reflection effect is rather small, i.e. the light curves are almost flat outside the eclipse.

For a given inclination, i , a single eclipse will give an accurate measurement of the radii of the stars relative to their separation, i.e. $r_{\text{WD}} = R_{\text{WD}}/a$ and $r_{\text{M}} = R_{\text{M}}/a$, where a is the separation of the stars and R_{WD} , R_{M} are the radii of the white dwarf and the M dwarf, respectively. Additionally, the depth of the eclipse gives an accurate measurement of the luminosity ratio, l_{λ} , at the effective wavelength of the light curve, λ . Equally good fits to the eclipse can be found for a wide range of i values. The shape of the M dwarf is accurately determined by an equipotential surface in the Roche potential, which is slightly non-spherical. This gives rise to an ellipsoidal effect with an amplitude of about 2 per cent in the I -band light curve. The amplitude of the ellipsoidal effect varies strongly with r_{M} and the predicted value of r_{M} increases as i decreases, so we have enough information in the u' -band and I -band light curves to measure r_{WD} , r_{M} and i .

We first measured the values of r_{WD} and r_{M} as a function of i from the u' -band light curve using the simple model of uniform circular discs described in Section 3.1. We included data obtained on the nights of 2002 May 24 and 2002 May 25 in the fit after first normalizing the data using a straight-line fit to the data outside of eclipse. The results are plotted in Fig. 9. We used the slightly more advanced light-curve model EBOP (Nelson & Davis 1972; Popper & Etzel 1981) to investigate the effect of limb-darkening on the values of r_{WD} and r_{M} derived; we found that these radii change by less than 0.1 per cent if limb-darkening is included in the model.

We used a simple model to calculate the semi-amplitude of the ellipsoidal effect in the I -band light curve, ΔI . The model creates a grid of points over an equipotential surface in the Roche potential. The observed flux as a function of phase is then calculated

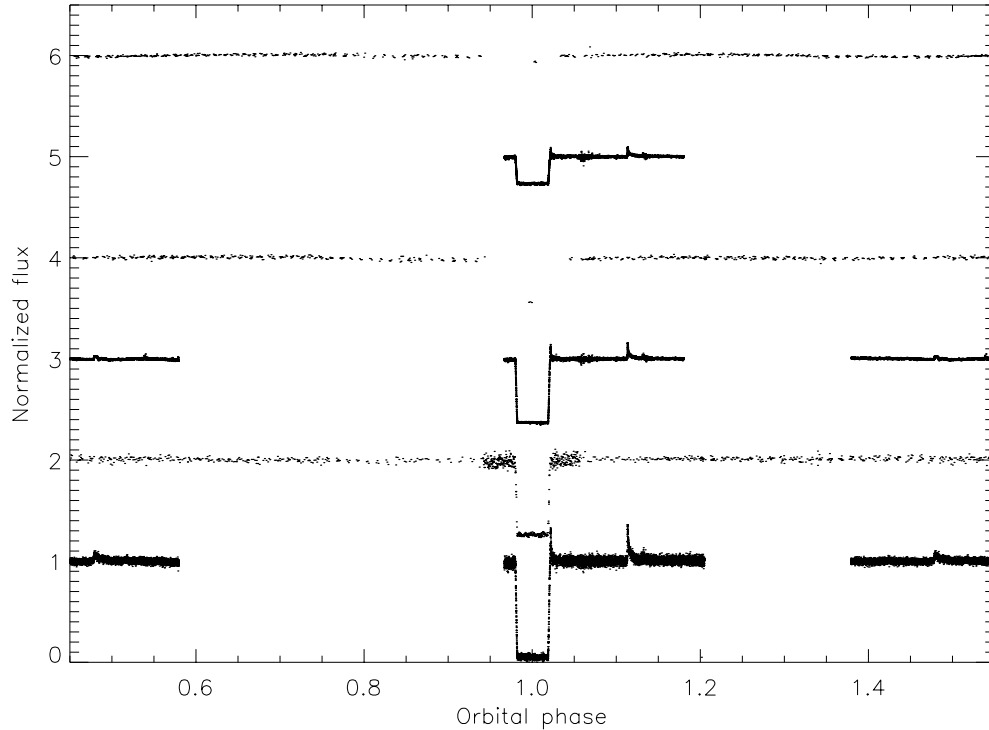


Figure 8. The light curves of RX J2130.6+4710 with the following filters (bottom to top); u' , B , g' , V , r' and I . The light curves have been normalized to the mean out-of-eclipse values and offset by 1.0 for clarity. The data for the u' , g' and r' filters around the primary eclipse were obtained on the night of 2002 May 17 and clearly show two flares. Data at other phases for the u' and g' bands were taken in poor seeing conditions on the night of 2003 November 13 and also shows two flares.

by numerical integration of the apparent surface brightness over the points visible at each phase. The apparent surface brightness over the star includes the effects of gravity darkening and limb-darkening. We calculated the value of ΔI as a function of i for linear limb-darkening coefficients of 0.63 and 0.72, which covers the range of values given in the tabulations of Claret (2000) for model stellar atmospheres with $T_{\text{eff}} = 3500$ K. The gravity darkening exponent was fixed at its standard value of 0.08. The effect of gravity darkening is to make the light curve slightly fainter at phase 0 than phase 0.5. To calculate ΔI we used the semi-amplitude calculated from the flux at phase 0.5 because the data at phase 0 are affected by the eclipse of the white dwarf, although the difference is very small for the amplitudes we are dealing with in this case. We also ignore the effect of the light from the white dwarf when we calculate ΔI , so a small correction for this contribution to the flux has to be made before comparing the predicted and observed values of ΔI . The predicted values of ΔI as a function of i are shown in Fig. 9.

The measurement ΔI is complicated by the asymmetry of the I -band light curve, e.g. the minimum of the light curve does not occur at phase 0.5. We assume that this is due to the presence of spots on the surface of the M dwarf. This is not an unreasonable assumption given that this is a rapidly rotating M dwarf that is known to show flares (Fig. 8). To model the effect of these spots on the light curve, we assumed that there are two spots that cause dips in the light curve described by the functions $A_j[1 + \cos(\phi - \phi_j)]/2$, $j = 1, 2$, which are restricted to orbital phases $\phi_j \pm \pi/2$. We modelled the ellipsoidal effect with the function $-\Delta I \cos(2\phi)$ and also included a component for the reflection effect using the function $-A_{\text{ref}} \cos(\phi)$. We first formed the average of the observations in phase bins 0.02 wide and calculated the standard deviation of the mean of the data in

each bin. We then subtracted a constant to remove the contribution of the white dwarf to the measured flux and renormalized the data by its mean. The value of the constant is determined from the mean value of the observed flux during eclipse.

We then performed a weighted least-squares fit of the sum of the functions described above plus a constant to the phase-binned data excluding the data in eclipse to find optimum values of the parameters A_1 , A_2 , ϕ_1 , ϕ_2 , ΔI , A_{ref} and the constant. The resulting fit and the phase-binned data are shown in Fig. 10. With so many parameters, there will clearly be many solutions that give a good fit. In this case we are interested in finding the likely range of ΔI values that are reasonable given the observed light curve. To find the value of ΔI we attempted to fit the I -band light curve with the dips due to the spots centred near phases 0.4 and 0.9 so as to remove as much of the variability as possible using the spots alone. The parameters for this fit are shown in Table 7.

The I -band data and the radial velocity data for the M dwarf discussed in Section 3.3 were obtained simultaneously so the parameters for the dark spots we infer by modelling distortions to the light curve and radial velocity curve should be consistent. This is indeed the case for the phase of the distortion of the proposed spot with $\phi_1 \approx 0.4$, which is also responsible for the distortion to the radial velocity curve with $\phi_0 \approx 0.2$ since $\phi_1 \approx \phi_0 + \rho/2$. The radial velocity data near phase 0.8 are too sparse to confirm whether the value of $\phi_2 = 0.83$ for the second spot is reasonable. We can, in principle, check for consistency between the amplitudes of the distortions, but this is a less straightforward test (see ‘Discussion’ below). We can at least point out that the size of the distortions to the I -band light curves are about 2 per cent and that the distortion to the radial velocity curve is about 2 per cent of the equatorial rotational velocity of the M dwarf (51 km s^{-1}).

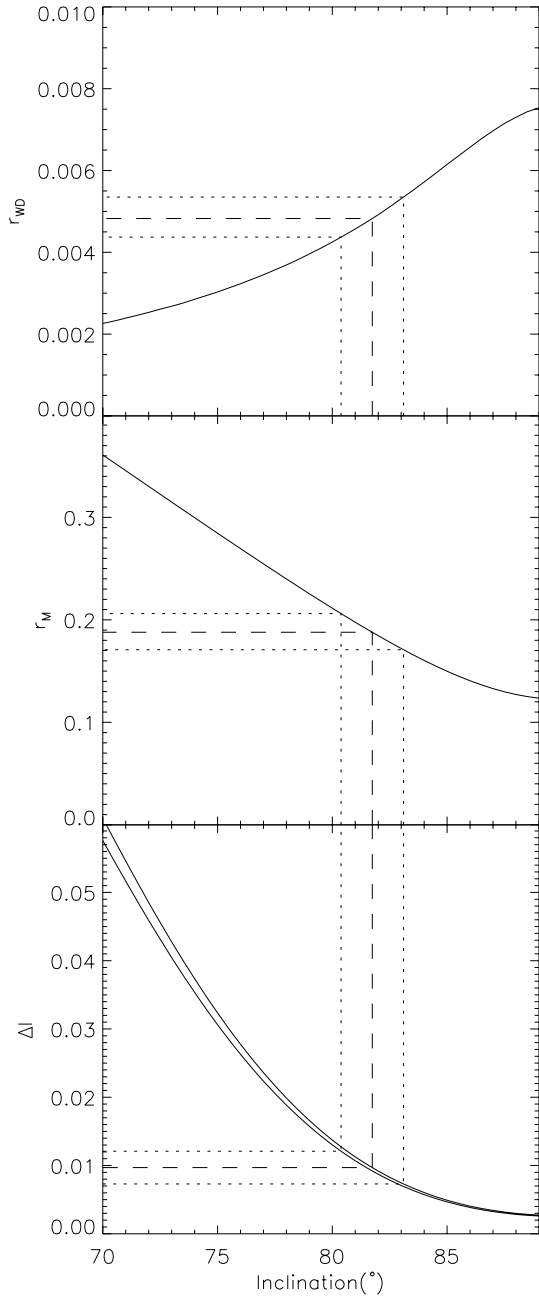


Figure 9. Upper panel: the optimum value of r_{WD} as a function of inclination from the least-squares fit to the u' -band light curve; middle panel: optimum value of r_{M} ; lower panel: the predicted semi-amplitude of the I -band light curve, ΔI , for two values of the limb darkening coefficient. The conversion of the observed value of ΔI to values of r_{WD} and r_{M} and their uncertainties are illustrated by dashed and dotted lines, respectively.

3.7 Masses and radii of the stars

From the lower panel of Fig. 9 we find that the observed value of $\Delta I = 0.0097 \pm 0.0024$ corresponds to an inclination of $i = (81.7 \pm 1.4)^\circ$. From the upper two panels we then find $r_{\text{WD}} = 0.0048 \pm 0.0005$ and $r_{\text{M}} = 0.188 \pm 0.018$. We combine these values with the combined spectroscopic orbit in Table 6 to derive the masses and radii for the stars given in Table 8. The positions of the stars in the mass–radius plane is compared with other white dwarfs and M dwarfs in Fig. 11.

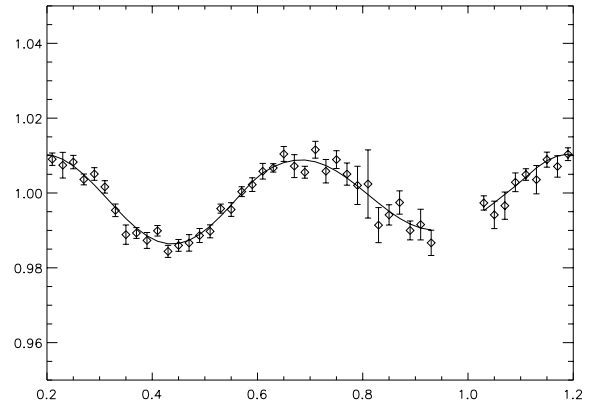


Figure 10. The phase-binned I -band light curve of RX J2130.6+4710 with a model fitted to two spot-like components, an ellipsoidal component and a reflection component.

Table 7. Parameters of the least-squares fit to the I -band light curve.

Parameter	Value
Constant	1.0103 ± 0.00053
ΔI	0.0097 ± 0.0024
A_{ref}	0.0010 ± 0.0009
A_1	0.0175 ± 0.0012
ϕ_1	0.369 ± 0.023
A_2	0.0143 ± 0.0021
ϕ_2	0.833 ± 0.022
χ^2	40.86
N	46

Table 8. The masses, radii and effective temperatures of the stars in RX J2130.6+4710.

Parameter	White dwarf	M dwarf
Mass (M_\odot)	0.554 ± 0.017	0.555 ± 0.023
Radius (R_\odot)	0.0137 ± 0.0014	0.534 ± 0.053
T_{eff} (K)	$18\,000 \pm 1000$	3200 ± 100^a

^aBased on our estimate of the spectral type and the calibration of Leggett (1992).

3.8 The effective temperature of the white dwarf

We compared the spectra of RX J2130.6+4710 with a grid of synthetic spectra calculated from pure hydrogen model atmospheres to estimate the effective temperature, T_{eff} , of the white dwarf.

These have been generated with the latest versions of the plane-parallel, hydrostatic, non-local thermodynamic equilibrium (non-LTE) atmosphere and spectral synthesis codes TLUSTY v.200 (Hubeny 1988; Hubeny & Lanz 2003) and SYNPEC v.48 (Hubeny, Stefl & Harmanec 1985). All calculations include a full treatment of line blanketing and use a state-of-the-art model hydrogen atom incorporating the eight lowest energy levels and one super-level extending from $n = 9$ to $n = 80$. During the calculation of the model structure, lines of the Lyman and Balmer series are treated by means of an approximate Stark profile. However, as we use the Balmer lines to determine the effective temperature and surface gravity of the white dwarf, it is important that we employ the best available line broadening data. Therefore, during the spectral synthesis step,

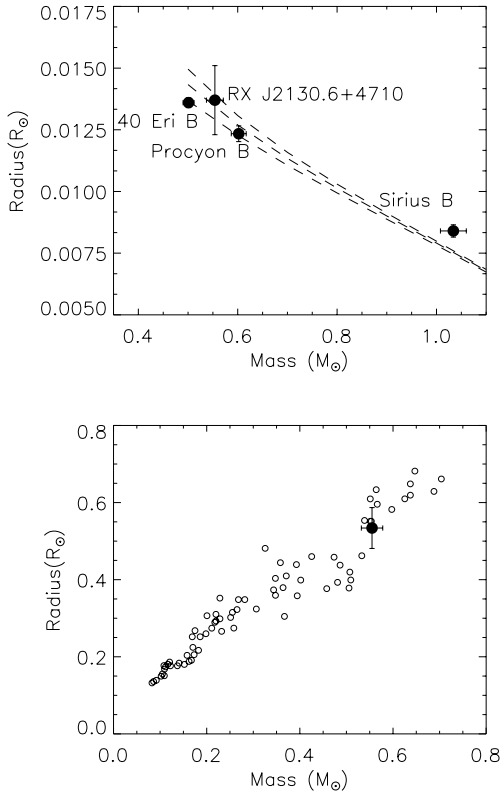


Figure 11. Upper panel: the white dwarf component of RX J2130.6+4710 in the mass–radius plane compared with other white dwarfs as labelled and the models of Benvenuto & Althaus (1999) for effective temperatures of 700, 17 000 and 24 790 K. Lower panel: the M-dwarf component of RX J2130.6+4710 in the mass–radius plane (filled circle) compared with other M dwarfs (open circles) taken from Clemens et al. (1998).

detailed profiles for the H I lines are calculated from the Stark broadening tables of Lemke (1997). We calculated synthetic spectra for model atmospheres over a range $15\,000\text{ K} < T_{\text{eff}} < 65\,000\text{ K}$ in steps of 5000 K and surface gravities in the range $6.5 < \log g < 8.5$ in steps of 0.5 ($\log g$ in cgs units).

In order to compare the spectra of RX J2130.6+4710 with the model spectra, we first had to remove the contribution of the M dwarf from the spectra. The spectra were normalized by a constant value determined from the mean flux around 4600 \AA . We interpolated the spectra on to a uniform wavelength grid of 2760 pixels over the wavelength range $3780\text{--}5105\text{ \AA}$. We formed the average of spectra in groups taken at the same orbital phase to within 0.04 phase units. The phase ranges were chosen such that spectrum of RX J2130.6+4710 taken at mid-eclipse was in a group by itself. We calculated a scaling factor to apply to the mid-eclipse spectrum prior to subtracting it from each of the 24 phase-binned spectra by measuring the ratio of fluxes either side of the band head near 4954 \AA and the depth of the absorption feature near 4226 \AA . The scaling factor calculated was typically 0.25 at 4226 \AA and 0.36 at 4954 \AA . We multiplied the mid-eclipse spectrum by a linear function of wavelength fitted to these values prior to shifting it to account for the radial velocity then subtracting it from the phase-binned spectra.

We convolved the synthetic spectra with a Gaussian function to account for the resolution of the observed spectra and then interpolated the synthetic spectra on to the same wavelength grid as the phase-binned spectra. We were then able to compare the synthetic and observed spectra by calculating the χ^2 statistic for each combi-

nation of observed and synthetic spectra. We did this separately for each Balmer line after applying a linear normalization calculated from the flux in the line wings to all the spectra. We excluded from the calculation of χ^2 a region $\pm 100\text{ km s}^{-1}$ wide centred on the Balmer emission lines from the M dwarf, the Ca II H and K emission lines and an emission line near 3905.5 \AA which may be due to Si I.

For 20 of the phase-binned spectra, the synthetic spectrum that gave the lowest value of χ^2 was calculated from a model atmosphere with $T_{\text{eff}} = 20\,000\text{ K}$, $\log g = 8.0$. There is good agreement between the value of $\log g$ derived from fitting these spectra and the value calculated from the measured mass and radius, i.e. $\log g = 7.93^{+0.07}_{-0.09}$. Therefore, we created synthetic spectra corresponding to a range $15\,000\text{ K} < T_{\text{eff}} < 20\,000\text{ K}$ in steps of 1000 K and surface gravities of $\log g = 7.93, 7.84$ and 8.00 by interpolation over the synthetic spectra calculated from the model atmospheres. We calculated the χ^2 statistic for these interpolated spectra as before. We found that 17 of the spectra were best fitted by model spectra with $T_{\text{eff}} = 18\,000\text{ K}$, $\log g = 7.84$ or $T_{\text{eff}} = 17\,000\text{ K}$, $\log g = 7.99$. These model spectra and a typical phase binned spectrum are shown in Fig. 12. The remaining seven spectra were best fitted by spectra within one grid-step of these two models. The quality of fits for spectra taken at phases from 0 to 0.5 judged by eye and from the value of χ^2 is very good. The fits are not so good in the other half of the orbit if judged by the value of χ^2 (reduced χ^2 values ≈ 1.5). There is no reason for this that is obvious from an inspection of the fits, but it is probably due to a combination of inaccurate subtraction of the M-dwarf spectrum and inaccuracies in the flux calibration. The spectra in the phases range 0 to 0.5 tend to be fitted best by spectra with $T_{\text{eff}} = 18\,000\text{ K}$. Therefore, we adopt an effective temperature of $T_{\text{eff}} = 18\,000\text{ K}$ for the white dwarf in RX J2130.6+4710 and estimate that the uncertainty in this estimate is about 1000 K.

4 DISCUSSION

We can estimate the distance and reddening to RX J2130.6+4710 from its effective temperature and our B and V photometry. From the tabulations of Bergeron, Wesemael & Beauchamp (1995) we estimate that the white dwarf in RX J2130.6+4710 has an intrinsic colour $(B-V)_0 = 0.00 \pm 0.02$ and an absolute V magnitude, $M_V = 11.0 \pm 0.1$. From the depths of the eclipses in the B and V bands combined with the photometry in Table 2 we can estimate apparent magnitudes for the white dwarf of $V = 15.05 \pm 0.1$, $(B-V) = 0.2 \pm 0.14$. From these values we estimate $E(B-V) = 0.2 \pm 0.15$, $(m-M) = 4.65 \pm 0.5$ and a distance to RX J2130.6+4710 of 85 ± 20 parsec.

The distance to HD 204906 is known to be 82 ± 5 parsec from its Hipparcos parallax (Perryman et al. 1987). It would be fortunate if RX J2130.6+4710 could be shown to be physically related to HD 204906 because we could then measure accurate absolute magnitudes for the stars in this binary. Unfortunately, the measured radial velocity for HD 204906 is $34.8 \pm 1.4\text{ km s}^{-1}$ (Sandage & Fouts 1987), which is very different from the value of $\gamma_M = 15.3 \pm 0.7$ we have measured. This suggests that HD 204906 and RX J2130.6+4710 are not physically related. One possibility that should be investigated is whether HD 204906 is itself a binary star.

The M dwarf in RX J2130.6+4710 shows all the characteristics of a magnetically active star, i.e. soft X-ray emission, Balmer emission lines, flares and spots. We have attempted some crude modelling of the distortions to the radial velocity and light curves to account for these distortions. In reality, these spots are likely to be a complex

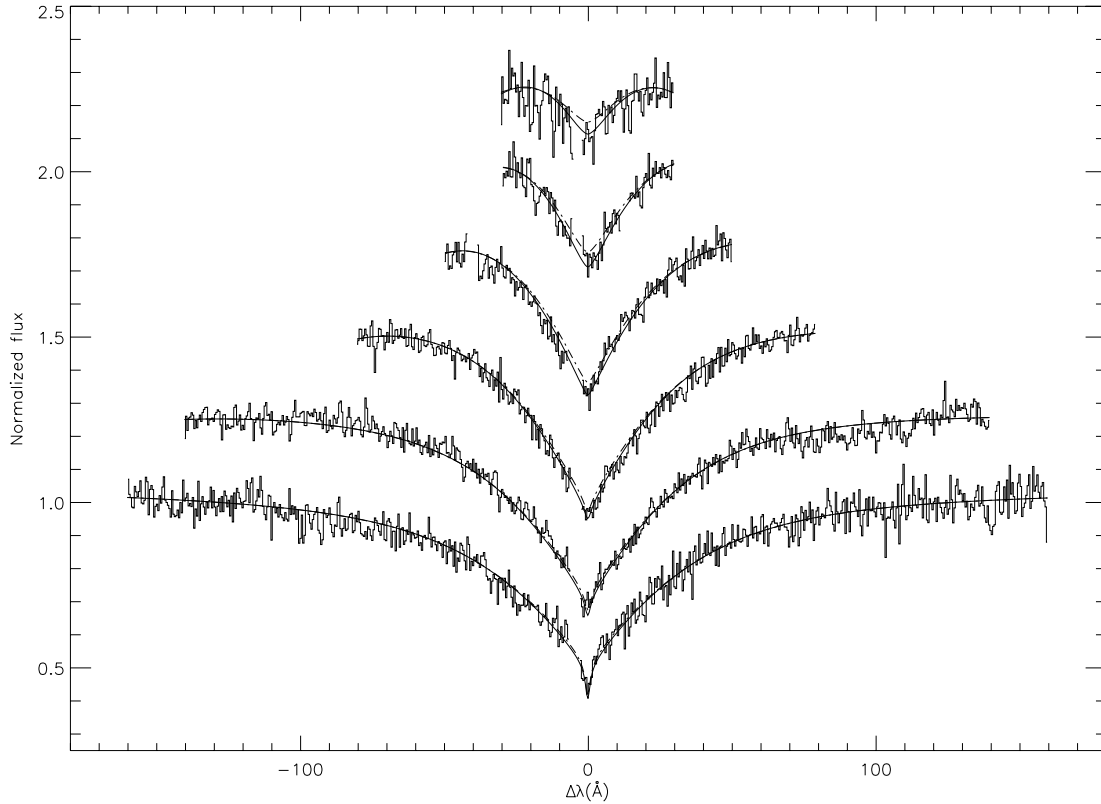


Figure 12. A typical phase-binned spectrum of the white dwarf in RX J2130.6+4710 plotted in sections offset by 0.25 around each Balmer line. The solid and dashed lines are synthetic spectra from model atmospheres with $T_{\text{eff}} = 18\,000$ K, $\log g = 7.84$ and $T_{\text{eff}} = 17\,000$ K, $\log g = 7.99$, respectively.

pattern of dark regions with variations in the local temperature and the emergent spectrum. This pattern of dark regions can be approximated using models with circular spots, each with its own position (latitude and longitude), physical size and temperature. Modelling the two spots we have used to model the *I*-band light curve would therefore require eight free parameters plus some model for how the emergent spectrum depends on local temperature and viewing angle. This is not warranted given the quality of our data. Further observations of RX J2130.6+4710 with improved phase coverage and resolution could be used to study the pattern of active regions on the surface of the M dwarf and the evolution of this pattern using techniques such as Doppler imaging (Rice 2002) or monitoring of the light curve. Such studies would benefit from the independent determinations of the rotational period of the star (assuming it is the same as the orbital period) the inclination of the star and the radius of the star presented here. This would, for example, allow a comparison of the rotational period derived from a Fourier analysis of the light curve excluding eclipses with the orbital period in order to look for asynchronous rotation in the M dwarf. Monitoring of the eclipse times will then allow a further test of the mechanism proposed by Applegate (1992) to explain period changes in binaries similar to RX J2130.6+4710 such as V471 Tau. Indeed, the orbital periods of V471 Tau and RX J2130.6+4710 are very similar, so comparison of the results for these two stars will provide observational evidence for the way in which Applegate’s mechanism depends on the mass of the magnetically active star.

In principle, a measurement of the depth of the secondary eclipse in RX J2130.6+4710 would allow a much more accurate determination of the masses and radii of the stars. Unfortunately, the predicted secondary eclipse depth is 7 milli-magnitudes or less. This

will be very difficult to measure given the proximity of HD 204906 to RX J2130.6+4710 and the distortions to the light curve due to spots and flares. A more straightforward way to improve the accuracy of the masses and radii will be to obtain improved spectroscopy, both in terms of resolution and signal-to-noise, and to obtain a light curve at near infrared wavelengths where the measurement of the ellipsoidal effect will be less affected by star spots. High-resolution spectroscopy at wavelengths of 3800–4000 Å may reveal sharp metal lines due to accretion of metals on to the surface of the white dwarf from the stellar wind of the M dwarf (Zuckermann et al. 2003). These lines, if present, would allow the measurement of accurate radial velocities for the white dwarf and thus an accurate measurement of its gravitational redshift.

The spectral type of the M dwarf in RX J2130.6+4710 is estimated to be M3.5Ve or M4Ve and its mass is $0.555 \pm 0.023 M_{\odot}$. This combination of mass and spectral type is not consistent with the calibration of Leggett (1992) for M stars in the galactic disc. A typical M3.5V in the galactic disc has a mass of about 0.2–0.3 M_{\odot} . An M-type star in the galactic disc with a mass of 0.55 M_{\odot} usually has a spectral type in the range M0V – M2V. This discrepancy may be due to an inaccurate estimate of the spectral type for the M dwarf caused by using a limited spectral range with few features sensitive to spectral type and comparing this spectrum with those of stars that are not standard stars for the spectral class. A much more reliable estimate of the spectral type of the M dwarf in RX J2130.6+4710 should be made using a spectrum taken during the eclipse covering the TiO bands in the regions 6000 Å – 9000 Å. By contrast, the observed value of $(J-H) = 0.63$ is negligibly affected by the presence of the white dwarf and is typical for M-type stars in the galactic disc with a mass of 0.55 M_{\odot} .

We have investigated the past and future evolution of RXJ2130.6+4710 using the analysis described by Schreiber & Gänsicke (2003). The cooling age, t_{cool} , of RXJ2130.6+4710 derived by interpolating the cooling tracks of Wood (1995) is $\log(t_{\text{cool}}/y) = 7.85$. This is the time since RXJ2130.6+4710 emerged from the common-envelope phase, at which time the orbital period is estimated to have been 0.53–0.6 d depending on the prescription used to model the angular momentum loss due to a magnetic stellar wind in this interval. The continued loss of angular momentum will shrink the Roche lobe of the M dwarf to the point where mass transfer will start from the M dwarf to the white dwarf through the inner Lagrangian point. This will occur at an orbital period $P_{\text{sd}} = 0.185$ d. Our estimate of the time before Roche lobe overflow occurs, t_{sd} , also depends on the prescription for angular momentum loss used and varies from $\log(t_{\text{sd}}/y) = 8.1$ to $\log(t_{\text{sd}}/y) = 9.6$. In either case, the time taken is less than a Hubble time so RXJ2130.6+4710 can properly be described as a pre-cataclysmic variable star (pre-CV) in the sense defined by Schreiber & Gänsicke. The value of P_{sd} for RXJ2130.6+4710 is well above the period gap for CVs and is second only to V471 Tau among the systems compiled by Schreiber & Gänsicke. This implies that RXJ2130.6+4710 is a member of the group of the rare progenitors of long orbital period CVs.

ACKNOWLEDGMENTS

The research reported in this paper was based on observations made with the William Herschel, Isaac Newton and Jacobus Kapteyn telescopes operated on the island of La Palma by the Royal Greenwich Observatory in the Spanish Observatorio del Roque de los Muchachos of the Instituto de Astrofísica de Canarias. PFLM and LMR were supported by a PPARC post-doctoral grant. We would like to thank Romano Corradi for his prompt and informative reply to our query regarding the timing accuracy of data from the ING. This research has made use of the SIMBAD database, operated at CDS, Strasbourg, France. We thank an anonymous referee for comments and suggestions regarding the modelling of distortions to the light curve and radial velocity curve.

REFERENCES

Applegate J. H., 1992, *ApJ*, 385, 621
 Benvenuto O. G., Althaus L. G., 1999, *MNRAS*, 303, 30
 Bergeron P., Wesemael F., Beauchamp A., 1995, *PASP*, 107, 1047
 Claret A., 2000, *A&A*, 363, 1081
 Clemens J. C., Reid I. N., Gizis J. E., O'Brien M. S., 1998, *ApJ*, 496, 352

Dhillon V. S., Marsh T. R., 2001, *New Ast. Rev.*, 45, 91
 Grabowski B., Halenka J., Madej J., 1987, *ApJ*, 313, 750
 Harris D. E. et al., 1994, *EINSTEIN Observatory Catalog of IPC X-ray Sources*, SAO HEAD CD-ROM Series I (Einstein), Nos 18–36
 Hawley S. L., Gizis J. E., Reid I. N., 1996, *AJ*, 112, 2799
 Hoard D. W., Wachter S., Clark L. L., Bowers T. P., 2002, *ApJ*, 565, 511
 Hubeny I., 1988, *Computer Physics Comm.*, 52, 103
 Hubeny I., Lanz T., 2003, in Hubeny I., Mihalas D., Werner K., eds, *ASP Conf. Ser. 288, Stellar Atmosphere Modeling*. Astron. Soc. Pac., San Francisco, p. 117
 Hubeny I., Stefl S., Harmanec P., 1985, *Bull. Astron. Inst. Czechosl.*, 36, 214
 Iben I., Livio M., 1993, *PASP*, 105, 1373
 Jaschek C., Jaschek M., 1987, *The Classification of Stars*. Cambridge Univ. Press
 Landolt A. U., 1992, *AJ*, 104, 340
 Leggett S. K., 1992, *ApJS*, 82, 351
 Lemke M., 1997, *A&AS*, 122, 285
 Marsh T. R., 1989, *PASP*, 101, 1032
 Motch C. et al., 1991, *A&A*, 246, L24
 Motch C., Guillout P., Haberl F., Pakull M. W., Peitsch W., Reinsch K., 1997, *A&A*, 318, 111
 Naylor T., 1998, *MNRAS*, 296, 339
 Nelson B., Davis W. D., 1972, *ApJ*, 174, 617
 Nidever D. L., Marcy G. W., Butler R. P., Fischer D. A., Vogt S. S., 2002, *ApJS*, 141, 503
 Oke J. B., 1990, *J*, 99, 1621
 Perryman M. A. C. et al., 1997, *A&A*, 323, L49
 Popper D. M., Etzel P. B., 1981, *AJ*, 86, 102
 Press W. H., Teukolsky S. A., Vetterling W. T., Flannery B. P., 1992, *Numerical Recipes in FORTRAN*, 2nd edn. Cambridge Univ. Press, Cambridge
 Reid I. N., Hawley S. L., Gizis J. E., 1995, *AJ*, 110, 1838
 Rice J. B., 2002, *AN*, 323, 220
 Ritter H., Kolb U., 1998, *A&AS*, 129, 83
 Sandage A., Fouts G., 1987, *AJ*, 93, 592
 Schneider D. P., Young P., 1980, *ApJ*, 238, 946
 Schreiber M. R., Gänsicke B. T., 2003, *A&A*, 406, 305
 Thompson R. J., Shelton R. G., Arming C. A., 1998, *AJ*, 115, 2587
 Trümper J., 1983, *Adv. Space. Res.*, 2, 241
 Wallace P. T., 2000, *SLALIB Programmer's Manual*, Starlink User Note 67.61, CCLRC/Rutherford Appleton Laboratory (<http://star-www.rl.ac.uk/star/docs/sun67.htx/sun67.html>)
 Wenger M. et al., 2000, *A&AS*, 143, 9
 Wood M. A., 1995, in Koester D., Werner K., *Lecture Notes in Phys. Vol. 443, White Dwarfs*. Springer, Heidelberg, p. 41
 Zuckerman B., Koester D., Reid I. N., Hüensch M., 2003, *ApJ*, 596, 477

This paper has been typeset from a $\text{\TeX}/\text{\LaTeX}$ file prepared by the author.